

A transit timing variation observed for the long-period extremely low density exoplanet HIP 41378 f

Edward M. Bryant^{1,2*}, Daniel Bayliss^{1,2}, Alexandre Santerne³, Peter J. Wheatley^{1,2}, Valerio Nascimbeni⁴, Elsa Ducrot⁵, Artem Burdanov^{5,6}, Jack S. Acton⁷, Douglas R. Alves⁸, David R. Anderson^{1,2}, David J. Armstrong^{1,2}, Supachai Awiphan⁹, Benjamin F. Cooke^{1,2}, Matthew R. Burleigh⁷, Sarah L. Casewell⁷, Laetitia Delrez^{5,10,11}, Brice-Olivier Demory¹², Philipp Eigmüller¹³, Akihiko Fukui^{14,15}, Tianjun Gan¹⁶, Samuel Gill^{1,2}, Michael Gillon²⁹, Michael R. Goad⁷, Thiam-Guan Tan¹⁷, Maximilian N. Günther¹⁸, Bronwen Hardee¹⁹, Beth A. Henderson⁷, Emmanuel Jehin¹⁰, James S. Jenkins^{8,20}, Molly Kosiarek²¹, Monika Lendl¹¹, Maximiliano Moyano²², Catriona A. Murray²³, Norio Narita^{15,24,25,26}, Prajwal Niraula⁶, Caroline E. Odden²⁷, Enric Palle^{15,28}, Hannu Parviainen^{15,28}, Peter P. Pedersen²³, Francisco J. Pozuelos^{29,10}, Benjamin V. Rackham^{6,8}, Daniel Sebastian³⁰, Chris Stockdale³¹, Rosanna H. Tilbrook⁷, Samantha J. Thompson²³, Amaury H.M.J. Triaud³⁰, Stéphane Udry¹¹, Jose I. Vines⁸, Richard G. West^{1,2}, Julien de Wit⁶

¹Dept. of Physics, University of Warwick, Gibbet Hill Road, Coventry CV4 7AL, UK

²Centre for Exoplanets and Habitability, University of Warwick, Gibbet Hill Road, Coventry CV4 7AL, UK

³Aix Marseille Univ, CNRS, CNES, LAM, Marseille, France

⁴INAF - Osservatorio Astronomico di Padova, Vicolo dell'Osservatorio 5, I-35122 Padova, Italy

⁵Astrobiology Research Unit, Université de Liège, Allée du 6 Août 19C, B-4000 Liège, Belgium

⁶Department of Earth, Atmospheric and Planetary Science, Massachusetts Institute of Technology, 77 Massachusetts Avenue, Cambridge, MA 02139, USA

⁷School of Physics and Astronomy, University of Leicester, Leicester, LE1 7RH, UK

⁸Departamento de Astronomía, Universidad de Chile, Casilla 36-D, Santiago, Chile

⁹National Astronomical Research Institute of Thailand, 260 Moo 4, Donkaew, Mae Rim, Chiang Mai, 50180, Thailand

¹⁰Space Sciences, Technologies and Astrophysics Research (STAR) Institute, Université de Liège, 19C Allée du 6 Août, 4000 Liège, Belgium

¹¹Observatoire Astronomique de l'Université de Genève, Chemin Pegasi 51, Versoix, Switzerland

¹²University of Bern, Centre for Space and Habitability, Gesellschaftsstrasse 6, 3012 Bern, Switzerland

¹³Institute of Planetary Research, German Aerospace Center, Rutherfordstrasse 2, 12489 Berlin, Germany

¹⁴Department of Earth and Planetary Science, Graduate School of Science, The University of Tokyo, 7-3-1 Hongo, Bunkyo-ku, Tokyo 113-0033, Japan

¹⁵Instituto de Astrofísica de Canarias (IAC), 38205 La Laguna, Tenerife, Spain

¹⁶Department of Astronomy and Tsinghua Centre for Astrophysics, Tsinghua University, Beijing 100084, China

¹⁷Perth Exoplanet Survey Telescope (PEST)

¹⁸Department of Physics, and Kavli Institute for Astrophysics and Space Research, Massachusetts Institute of Technology, Cambridge, MA 02139, USA

¹⁹Department of Earth and Planetary Sciences, University of California, Santa Cruz, CA 95064, USA

²⁰Centro de Astrofísica y Tecnologías Afines (CATA), Casilla 36-D, Santiago, Chile

²¹Department of Astronomy and Astrophysics, University of California, Santa Cruz, CA 95064, USA

²²Instituto de Astronomía, Universidad Católica del Norte, Angamos 0610, 1270709, Antofagasta, Chile

²³Astrophysics Group, Cavendish Laboratory, J.J. Thomson Avenue, Cambridge CB3 0HE, UK

²⁴Komaba Institute for Science, The University of Tokyo, 3-8-1 Komaba, Meguro, Tokyo 153-8902, Japan

²⁵JST, PRESTO, 3-8-1 Komaba, Meguro, Tokyo 153-8902, Japan

²⁶Astrobiology Center, 2-21-1 Osawa, Mitaka, Tokyo 181-8588, Japan

²⁷Phillips Academy Observatory, Phillips Academy, Andover MA USA

²⁸Departamento de Astrofísica, Universidad de La Laguna (ULL), 38206, La Laguna, Tenerife, Spain

²⁹Astrobiology Research Unit, Université de Liège, 19C Allée du 6 Août, 4000 Liège, Belgium

³⁰School of Physics & Astronomy, University of Birmingham, Edgbaston, Birmingham B15 2TT, United Kingdom

³¹Hazelwood Observatory

Accepted 2021 April 2. Received 2021 March 31; in original form 2021 March 10

ABSTRACT

HIP 41378 f is a temperate $9.2 \pm 0.1 R_{\oplus}$ planet with period of 542.08 days and an extremely low density of $0.09 \pm 0.02 \text{ g cm}^{-3}$. It transits the bright star HIP 41378 ($V=8.93$), making it an exciting target for atmospheric characterization including transmission spectroscopy. HIP 41378 was monitored photometrically between the dates of 2019 November 19 and November 28. We detected a transit of HIP 41378 f with NGTS, just the third transit ever detected for this planet, which confirms the orbital period. This is also the first ground-based detection of a transit of HIP 41378 f. Additional ground-based photometry was also obtained and used to constrain the time of the transit. The transit was measured to occur 1.50 hours earlier than predicted. We use an analytic transit timing variation (TTV) model to show the observed TTV can be explained by interactions between HIP 41378 e and HIP 41378 f. Using our TTV model, we predict the epochs of future transits of HIP 41378 f, with derived transit centres of $T_{C,4} = 2459355.087^{+0.031}_{-0.022}$ (May 2021) and $T_{C,5} = 2459897.078^{+0.114}_{-0.060}$ (Nov 2022).

Key words: techniques: photometric – planets and satellites: gaseous planets – planets and satellites: detection – planets and satellites: individual: HIP 41378 f – stars: individual: HIP 41378

1 INTRODUCTION

The bright ($V=8.93$) F-type star HIP 41378 is known to host five transiting planets (Vanderburg et al. 2016), based on photometric data taken during campaign C5 of the *K2* mission (Howell et al. 2014). The outer most planet known in the system, HIP 41378 f only transited once during these observations. A second transit of HIP 41378 f was observed during *K2* campaign C18 and showed it to have a maximum possible orbital period of 1084.159 days (Becker et al. 2019). Extensive spectroscopic monitoring with HARPS by Santerne et al. (2019) revealed the true period of HIP 41378 f to be 542.08 days - half the possible maximum.

With a mass of $M_p = 12 \pm 3 M_{\oplus}$ and a radius of $R_p = 9.2 \pm 0.1 R_{\oplus}$, the low density of HIP 41378 f, combined with its cool temperature, makes it a particularly interesting target for atmospheric characterization. Using the system parameters from Santerne et al. (2019) we calculate a Transmission Spectroscopy Metric (TSM) for HIP 41378 f of 343 (Kempton et al. 2018), which shows HIP 41378 f to be very well suited to transmission spectroscopy follow-up. For these observations, a precise orbital ephemeris is needed. Despite the high quality *K2* data, with only two recorded transits there was previously no information regarding any transit timing variations (TTVs) of HIP 41378 f. In a multi-planet system, a planet with a long orbital period such as HIP 41378 f may experience large transit timing variations (TTVs) (eg. Agol et al. 2005; Kawahara & Masuda 2019). Since HIP 41378 f resides in near 2:1 and 3:2 mean motion resonances with planet e and d respectively, we may expect TTVs on the order of hours to days.

Ground-based photometric observations of the HIP 41378 system are needed to measure any TTVs to place additional constraints on the masses and orbital periods of planets in the HIP 41378 system. Monitoring the TTVs also has the potential to reveal other exoplanets in the system, and additionally will help predict future transit events for atmospheric characterisation. However, for a star with a magnitude of $V=8.93$ the field-of-view of most ground-based photometric facilities will often not include enough comparison stars of a similar brightness (Collins et al. 2018). In fact, for HIP 41378,

the nearest star with a GAIA G magnitude difference of less than 0.5 mag is 17 arcmin away (Gaia Collaboration et al. 2018).

2 PHOTOMETRIC OBSERVATIONS**2.1 NGTS**

The Next Generation Transit Survey (NGTS; Wheatley et al. 2018) is a photometric facility situated at ESO’s Paranal Observatory in Chile. It consists of twelve fully-robotic telescopes with 20 cm diameter apertures and wide fields-of-view of 8 square degrees. The dominant photometric noise sources in NGTS bright star light curves have been shown to be Gaussian and uncorrelated between the individual telescopes (Bryant et al. 2020). Combined with the wide field-of-view, this allows NGTS to use simultaneous observations with multiple telescopes to achieve high precision light curves of bright stars (Smith et al. 2020; Bryant et al. 2020).

HIP 41378 was observed with NGTS on the nights UT 2019 Nov 19, 24 and 25. On all nights, HIP 41378 was monitored using eleven NGTS telescopes, each using the custom NGTS filter (520–890 nm) and an exposure time of 10 seconds. Across all nights, a total of 23841 images were taken. The target was above an altitude of 30° for all the observations, and the observing conditions were good.

The NGTS data were reduced using a custom aperture photometry pipeline, which utilises the SEP Python library (Bertin & Arnouts 1996; Barbary 2016). The pipeline uses the GAIA DR2 catalogue (Gaia Collaboration et al. 2016, 2018) to automatically identify comparison stars that are similar in magnitude, colour and CCD position to HIP 41378 (for more details see Bryant et al. 2020). Comparison stars which are shown to display variability or high levels of photometric scatter are excluded from the reduction. The NGTS photometry is plotted in Figure 1.

2.2 SPECULOOS

HIP 41378 was observed by SPECULOOS (Search for habitable Planets Eclipsing ULtra-cOOl Stars; Burdanov et al. 2018; Gillon 2018; Delrez et al. 2018; Sebastian et al. 2021). It was observed from the SPECULOOS Southern Observatory (SSO) at Paranal, Chile on UT 2019 Nov 24 and from the SPECULOOS Northern Observatory

* E-mail: edward.bryant@warwick.ac.uk

† Juan Carlos Torres Fellow

‡ NSF Graduate Research Fellow

§ 51 Pegasi b Fellow

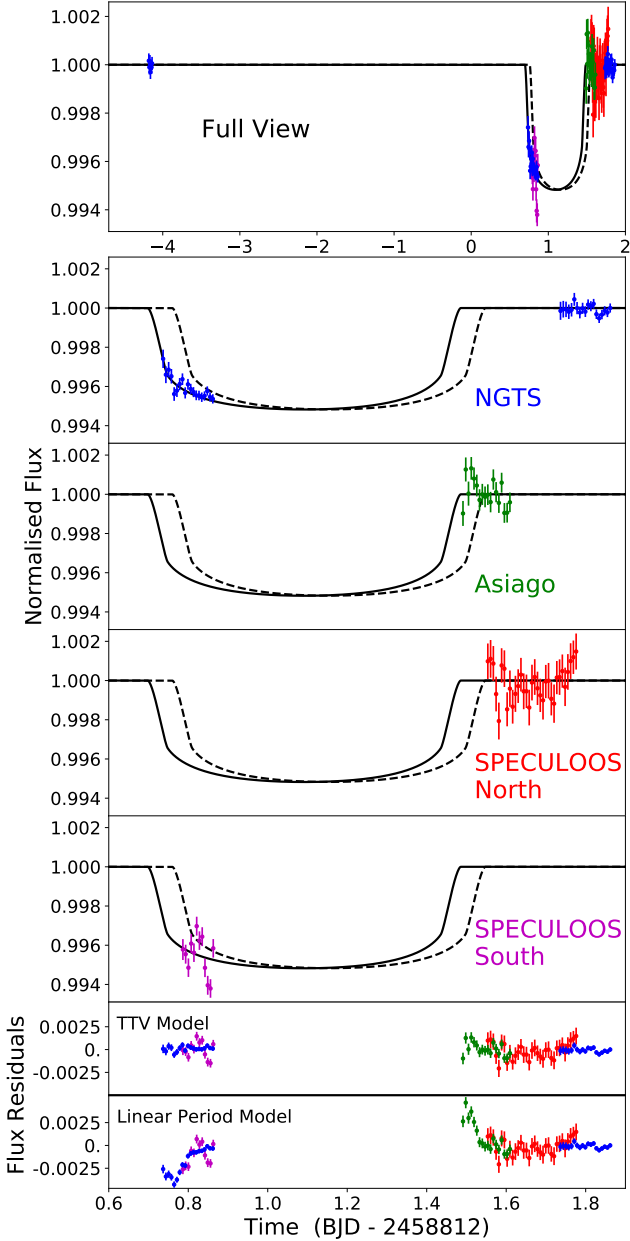


Figure 1. Ground-based relative time-series photometry of HIP 41378. All the photometric data included in the analysis are shown in the top panel. The individual datasets are presented in the following panels: NGTS (blue; second panel) showing a zoom in on the transit of HIP 41378f, ASIAGO (green; third panel), SNO (red; fourth panel) and SSO (magenta; fifth panel). All data are binned to 10 minutes. The predicted transit model of HIP 41378f from the K2 and HARPS data is given by the dashed black line, and the model from our sampling process is given by the solid black line. The residuals to the TTV model from our fitting are presented in the sixth panel and the residuals to the predicted linear period model from the two prior transits are presented in the bottom panel. We note that the colours used to denote the individual datasets are consistent across each panel. Note that we plot the detrended NGTS data and the relative flux offsets between the photometry obtained at different facilities were fit as free parameters during the modelling set out in Section 3.

(SNO) at the Teide Observatory on Tenerife, Spain on UT 2019 Nov 25. The SSO observations consists of 342 images obtained using the r' filter, an exposure time of 12 seconds, and a defocus of 300 steps to avoid saturation. SNO obtained 254 images using also the r' filter, with an exposure time of 12 seconds and a defocus of 300 steps. For each night of observation, the automatic SSO Pipeline (Murray et al. 2020) was used to reduce images and extract precise photometry. The SSO Pipeline is built upon the casutools software (Irwin et al. 2004) and performs automated differential photometry to mitigate ground-based systematics, including a correction for time-varying telluric water vapour. The SNO and SSO data are plotted in Figure 1.

2.3 Asiago Telescope

HIP 41378 was observed on the night UT 2019 Nov 25 using the 67/92-cm Schmidt telescope based at the Asiago Observatory in northern Italy, operated by the Italian National Institute of Astrophysics (INAF). A total of 301 images were obtained through the Sloan r filter under a good sky quality, using a constant exposure time of 30 seconds and defocusing the camera to minimize pixel-to-pixel systematic errors. The light curve was extracted by using a custom version of the STARSKY code, a pipeline to perform high-precision differential photometry originally developed for the TASTE project (Nascimbeni et al. 2011). The unbinned RMS is 2.0 mmag, the scatter being much larger at the beginning of the series due to the much higher airmass (1.97 for the first frame). All the time stamps were converted to the BJD-TDB system (Eastman et al. 2010). The Asiago data, binned over a 10-min time scale (rms: 825 ppm) are plotted in Figure 1 (green points). The Asiago data are plotted in Figure 1.

2.4 Photometric Transit Detection

The NGTS data shows a clear flux decrease which is consistent to the predicted transit depth and near to the predicted transit time. This flux decrease is clearly seen in the top two panels of Figure 1. We note that the NGTS photometry is of sufficient precision that an ingress occurring at the time predicted from the K2 and HARPS data would be robustly detected. The SSO and Asiago data are consistent with the change in transit time seen by NGTS, ruling out an on-time ingress and egress respectively. The SNO data rule out a late transit. With photometric coverage on three separate nights surrounding the transit event, we are confident that the flux offset seen in the NGTS data is a real signal. However the relative flux offsets between the data from the different facilities, including the offset of the SSO data, were fit independently as free parameters during the modelling detailed in Section 3. The combination of these four datasets gives us confidence that the transit occurred earlier than the prediction from the linear orbital ephemeris derived from the K2 and HARPS data (Santerne et al. 2019). This is the third transit of this planet to be detected and the first from the ground, with the other two being detected from data obtained by the K2 mission. The detection of this transit confirms the 542.08 day period predicted for this planet from K2 and HARPS data (Santerne et al. 2019).

2.5 Additional Ground Based Photometry

Additional photometry for HIP 41378 was also obtained with various other ground-based facilities: PEST, LCO (CTIO), PROMPT-8 (CTIO), MUSCAT2 at Teide Observatory, Lick Observatory, Hazelwood Observatory, and Phillip’s Academy Observatory. Unfortu-

nately, due to poor observing conditions or a lack of suitable comparison stars, none of the data from these facilities had a photometric precision better than a threshold of 2 ppt-per-10 mins. As such we do not include these datasets in our analysis.

3 ANALYSIS

We jointly modelled the photometry from NGTS, ASIAGO, SSO and SNO in order to determine the time of transit centre for the November 2019 transit, $T_{C,3}$. Note we use the notation $T_{C,N}$ to refer to the time of transit centre for transit epoch N . The first transit of HIP 41378 f in K2 C5 is taken to occur at $T_{C,0}$. We generated a transit light curve template based on the parameters from [Vanderburg et al. \(2016\)](#), and using the period derived by [Santerne et al. \(2019\)](#). We performed an MCMC sampling process to model the ground-based photometric data. The free parameters used in the modelling were $T_{C,3}$, the limb darkening coefficients, the detrending coefficients for the NGTS data, and relative flux offset factors for the other datasets. Note that each NGTS single-telescope lightcurve was detrended against airmass independently from the other telescopes, and a single linear trend with time is applied to the entire NGTS multi-telescope light curve. We used a quadratic limb darkening profile, constraining the coefficients based on theoretically derived limb-darkening coefficients for the NGTS filter. The r' filter used for the SSO observations has a large amount of overlap with the wavelength range of the NGTS filter, and so the limb-darkening coefficients derived for the NGTS filter provide a good approximation for the SSO data. The precision of the SSO data also means that including an additional set of limb-darkening coefficients for the SSO data does not have an effect on the derived value of $T_{C,3}$. Therefore, we use the theoretical values of 0.315 ± 0.004 and 0.289 ± 0.001 , which were computed from the [Claret & Bloemen \(2011\)](#) tables, as Gaussian priors for the model for all datasets.

The sampling was performed using the Ensemble Sampler from [emcee \(Foreman-Mackey et al. 2013\)](#). We ran 70 chains for 10000 steps, following a burn-in phase of 2500 steps. The number of effective samples for each parameter ranged from 600000 to 800000, with the number of effective samples for $T_{C,3}$ was 698539.39784769. From this analysis, we obtained a transit time of $T_{C,3} = 2458813.0913 \pm 0.0046$, which is 1.50 ± 0.11 hours earlier than predicted. The best fit model from this analysis is shown in [Fig. 1](#) and the derived transit time variation is shown in [Fig. 2](#).

4 TTV ANALYSIS

Due to its anomalously low density, HIP 41378 f is an attractive target for atmospheric characterisation studies. As such, knowing the precise ephemerides for future transits is of high importance. Therefore, we use analytical TTV formulae from [Lithwick et al. \(2012\)](#) to predict the times of the upcoming transits of HIP 41378 f, in particular the next two transits in May 2021 and Nov 2022.

Of the planets already known in the system, the TTV signal of HIP 41378 f will be most affected by HIP 41378 d and HIP 41378 e. These two planets have masses of $M_d < 4.6M_{\oplus}$ and $M_e = 12 \pm 5M_{\oplus}$ ([Santerne et al. 2019](#)), and reside near to 2:1 and 3:2 mean motion resonances with HIP 41378 f, respectively. The amplitude of the TTVs of HIP 41378 f as a result of its interactions with HIP 41378 d and HIP 41378 e will depend strongly on M_d and M_e respectively. The interactions with HIP 41378 e are likely to dominate the TTV signal of HIP 41378 f since $M_e > M_d$ ([Santerne et al. 2019](#)) and

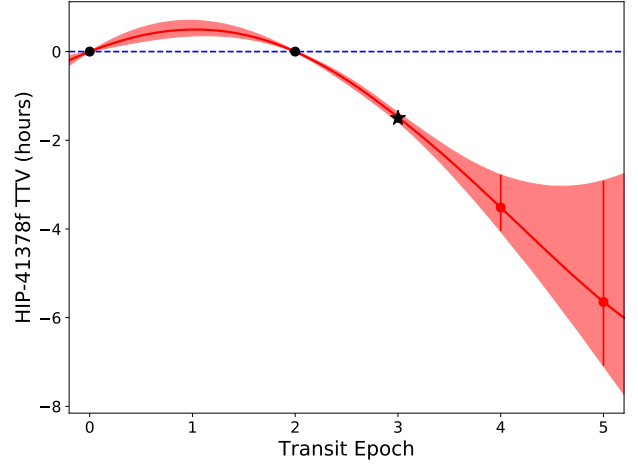


Figure 2. Transit times for HIP 41378 f. The black points give the T_C values for the two transits of HIP 41378 f observed by K2. The black star gives the new $T_{C,3}$ determined in this work. The 1σ errorbars on these values are plotted but are too small to be visible. The red points and errorbars give the predicted transit times for $T_{C,4}$ (May 2021) and $T_{C,5}$ (Nov 2022) and their respective 1σ uncertainties. The solid red line gives the median TTV signal from the TTV analysis (see Section 4), and the red shaded area gives the 1σ uncertainty on this signal. The TTV values are relative to the linear ephemeris based on the period from [Santerne et al. \(2019\)](#) of $T_0 = 2457186.91451$ and $P_f = 542.07975$ days, and this linear ephemeris is shown by the blue dashed line.

thus we consider solely the TTVs due to interactions between HIP 41378 f & e for the rest of this analysis. We note that neither HIP 41378 d nor HIP 41378 e were robustly detected by [Santerne et al. \(2019\)](#) in HARPS radial velocity measurements, and so they are only able to place loose constraints on the masses and periods of these planets. The constraints on the period of HIP 41378 e are derived from a combination of transit analyses and asteroseismic stellar constraints ([Santerne et al. 2019](#); [Lund et al. 2019](#)). Future monitoring of the TTVs of HIP 41378 f will allow us to place tighter independent constraints on the masses and periods of HIP 41378 d and HIP 41378 e.

We use the [Lithwick et al. \(2012\)](#) analytic formulae for TTV signals for planets in a near mean motion resonance to obtain the following equations for the amplitude, V , and super-period, P_{ttv} , for the TTV signal of HIP 41378 f as a result of its interactions with HIP 41378 e. These are

$$V = P_f \frac{M_{\text{pl},e}}{3\pi\Delta M_*} \left(-G + \frac{3}{2\Delta} (F e_e + G e_f) \right), \quad (1)$$

$$P_{\text{ttv}} = \frac{P_f}{3|\Delta|}, \quad (2)$$

where P_f is the mean linear orbital period of HIP 41378 f, $M_{\text{pl},e}$ and M_* are the masses of HIP 41378 e and HIP 41378, e_e and e_f are the orbital eccentricities of HIP 41378 e and HIP 41378 f respectively, and F and G are coefficients given in Table 3 of [Lithwick et al. \(2012\)](#). The Δ parameter is the normalized distance to resonance

$$\Delta = \frac{P_f}{P_e} \frac{2}{3} - 1, \quad (3)$$

where $P_e = 369 \pm 10$ days is the mean linear orbital period of HIP 41378 e. Using the planetary parameters given in Tab.1 of [Santerne et al. \(2019\)](#), we calculate values of $V = 1.3667$ days,

	$T_{C,4}$ (BJD TDB - 2450000)	$T_{C,5}$ (BJD TDB - 2450000)
Median	9355.087	9897.078
68%	9355.064 - 9355.118	9897.018 - 9897.192
95%	9355.032 - 9355.156	9896.910 - 9897.293
99%	9355.020 - 9355.205	9896.884 - 9897.455

Table 1. Confidence intervals for the predictions of $T_{C,4}$ and $T_{C,5}$.

and $P_{\text{ttv}} = 8757.577$ days. We note that the expected TTV signal from HIP 41378 e alone is enough to account for the TTVs observed in Section 2. Additional planets in the system are not required to explain the observations (nor do the observations rule them out).

With just three transit times, we cannot use TTV modelling to place any constraints on the masses and orbital eccentricities of the planets in the HIP 41378 system. Neither can we robustly refine the period of HIP 41378 e. However, we can combine the analytical TTV signals derived in Lithwick et al. (2012) with our knowledge of HIP 41378 f and e to predict the times of the next transits of HIP 41378 f. We do this using an MCMC sampling method, again using emcee Ensemble Sampler. The TTV model we use for this sampling is of the form

$$T_{C,N} = T_0 + P_f N + V \sin\left(\frac{2\pi P_f}{P_{\text{ttv}}}(N + \phi)\right) \quad (4)$$

where $T_{C,N}$ is the time of transit centre of the N^{th} transit, T_0 is a reference epoch and N is the transit epoch, such that $T_0 + P_f N$ is the mean linear ephemeris of HIP 41378 f, and ϕ is the phase shift of the TTV signal. The free parameters in this sampling are T_0 , P_f , ϕ , $M_{\text{pl},e}$, P_e , e_e and e_f . For the following parameters: $M_{\text{pl},e}$, P_e , e_e and e_f we impose Gaussian priors using the posterior values from Santerne et al. (2019). In this way, we explore the parameter space of TTV signals which can explain the transit times we observe for HIP 41378 f and are also physically plausible. For the sampling, we run 40 walkers each for 200000 steps as a burn-in, and then a following 50000 steps to explore the parameter space. The resultant predicted TTV signal from this sampling is given in Fig. 2. The median values of the resultant probability distributions for $T_{C,4}$ and $T_{C,5}$, as well as the 68%, 95%, and 99% confidence intervals, are provided in Table 1.

5 CONCLUSIONS

We detected a transit of HIP 41378 f on 2019 November 24 and 25, the first ever ground-based transit detection for this planet, primarily with data obtained using NGTS. As this is just the third ever transit of HIP 41378 f detected, we confirm the 542.08 day orbital period of this planet. This long orbital period makes HIP 41378 f the longest period planet to have a transit detected from the ground. The long transit duration (19 hours) makes detecting transits of HIP 41378 f challenging and makes photometric efforts with increased longitudinal coverage useful for recovering such transits. On the other hand, the fact that many of the observations taken for this particular effort were not able to be used to constrain the transit parameters highlights the value of photometric facilities like NGTS, when it comes to obtaining high precision photometry of bright stars like HIP 41378.

We found the transit to arrive 1.50 hours earlier than predicted from a linear extrapolation of the K2 transits (Vanderburg et al. 2016; Becker et al. 2019) and extensive spectroscopic monitoring (Santerne et al. 2019). Using analytic formulae for TTV signals from

Lithwick et al. (2012), we have shown that the TTV observed for HIP 41378 f can be explained solely through the interaction between HIP 41378 e and HIP 41378 f. Therefore, the presence of additional planets in the HIP 41378 system is not required to explain our observations. However our observations do not rule out the presence of additional planets. We predict that the next transit of HIP 41378 f will be centred on BJD 2459355.087 with a 99% confidence interval of 4.4 hours (2021 May 20), and the following transit will occur around BJD 2459897.078 with a 99% confidence interval of 13.7 hours (2022 Nov 13).

Both P_{ttv} and V depend strongly on the ratio of P_f/P_e . As P_f is well constrained by the available transits of HIP 41378 f, this results in the amplitude and period of the predicted TTV signal depending strongly on the orbital period of HIP 41378 e. The current large uncertainty on P_e combined with the shallow transit depth of just 1.5 mmag mean that detecting another transit of HIP 41378 e, especially with ground-based facilities, will be tough. However, doing so would greatly refine the predictions of the TTV signal of HIP 41378 f. Additionally, detecting the upcoming transits of HIP 41378 f will allow us to greatly refine the ephemeris of HIP 41378 e, due to the constraints that the improved measurements of V and P_{ttv} will place on P_e . The next transit of HIP 41378 e is predicted to have a centre time of $T_C = 2459356 \pm 60$ (UT 2021 May 21). HIP 41378 d is in near 4:3 mean-motion resonance with HIP 41378 e, and so based on our TTV models we expect HIP 41378 d to also experience large TTVs. Therefore, detecting transits of HIP 41378 d will further allow us to refine our TTV models and make better predictions for upcoming transits of HIP 41378 e. Using the sampling method from Section 4, we predict the next transit of HIP 41378 d to have a transit mid-point of $T_C = 2459393.13 \pm 0.59$ (2021 June 27).

With 6 planets in the HIP 41378 system, many of which reside near to mean-motion resonances, there are likely to be lots of interactions between the planets. With only a small number of transit detections for each of the outer three planets, a full dynamical analysis of the system is beyond the scope of this work. However, this robust transit detection of HIP 41378 f by NGTS and the discovery of significant TTVs in the system demonstrates that with future photometric monitoring we will be able to characterise the amplitude and super-period of the TTV signal of HIP 41378 f. This monitoring will enable us to place independent constraints on the masses, orbital periods, and eccentricities of the planets in this remarkable system.

ACKNOWLEDGEMENTS

Based on data collected by the NGTS project, the SPECULOOS network, the Asiago Observatory, the Las Cumbres Observatory global telescope network, the MuSCAT2 instrument, the PEST Observatory, the Lick Observatory, the Hazelwood Observatory, the Phillip's Academy Observatory, and the PROMPT-8 telescope at CTIO. For full acknowledgments for these facilities we refer the reader to the facility papers cited in this Letter.

MRK is supported by the NSF Graduate Research Fellowship, grant No. DGE 1339067. DJA acknowledges support from the STFC via an Ernest Rutherford Fellowship (ST/R00384X/1). MNG acknowledges support from MIT's Kavli Institute as a Juan Carlos Torres Fellow. NN is partly supported by JSPS KAKENHI Grant Numbers JP17H04574, JP18H01265 and JP18H05439, and JST PRESTO Grant Number JPMJPR1775, and a University Research Support Grant from the National Astronomical Observatory

of Japan (NAOJ). JSJ acknowledges support by FONDECYT grant 1201371, and partial support from CONICYT project Basal AFB-170002.

DATA AVAILABILITY

The NGTS, Asiago, SSO and SNO photometric data are available in the online supplementary material.

REFERENCES

- Agol E., Steffen J., Sari R., Clarkson W., 2005, *MNRAS*, **359**, 567
- Barbary K., 2016, *Journal of Open Source Software*, **1**, 58
- Becker J. C., et al., 2019, *AJ*, **157**, 19
- Bertin E., Arnouts S., 1996, *A&AS*, **117**, 393
- Bryant E. M., et al., 2020, *MNRAS*, **494**, 5872
- Burdanov A., Delrez L., Gillon M., Jehin E., 2018, SPECULOOS Exoplanet Search and Its Prototype on TRAPPIST. p. 130, doi:10.1007/978-3-319-55333-7_130
- Claret A., Bloemen S., 2011, *A&A*, **529**, A75
- Collins K. A., et al., 2018, *AJ*, **156**, 234
- Delrez L., et al., 2018, in Proc. SPIE. p. 107001I (arXiv:1806.11205), doi:10.1117/12.2312475
- Eastman J., Siverd R., Gaudi B. S., 2010, *PASP*, **122**, 935
- Foreman-Mackey D., Hogg D. W., Lang D., Goodman J., 2013, *PASP*, **125**, 306
- Gaia Collaboration et al., 2016, *A&A*, **595**, A2
- Gaia Collaboration Brown A. G. A., Vallenari A., Prusti T., de Bruijne J. H. J., Babusiaux C., Bailer-Jones C. A. L., 2018, preprint, (arXiv:1804.09365)
- Gillon M., 2018, *Nature Astronomy*, **2**, 344
- Howell S. B., et al., 2014, *PASP*, **126**, 398
- Irwin M. J., et al., 2004, in *Optimizing Scientific Return for Astronomy through Information Technologies*. SPIE, doi:10.1117/12.551449, <https://doi.org/10.1117/12.551449>
- Kawahara H., Masuda K., 2019, *AJ*, **157**, 218
- Kempton E. M. R., et al., 2018, *PASP*, **130**, 114401
- Lithwick Y., Xie J., Wu Y., 2012, *ApJ*, **761**, 122
- Lund M. N., et al., 2019, *AJ*, **158**, 248
- Murray C. A., et al., 2020, *MNRAS*, **495**, 2446
- Nascimbeni V., Piotto G., Bedin L. R., Damasso M., 2011, *A&A*, **527**, A85
- Santerne A., et al., 2019, arXiv e-prints, p. arXiv:1911.07355
- Sebastian D., et al., 2021, *A&A*, **645**, A100
- Smith A. M. S., et al., 2020, arXiv e-prints, p. arXiv:2002.05591
- Vanderburg A., et al., 2016, *ApJ*, **827**, L10
- Wheatley P. J., et al., 2018, *MNRAS*, **475**, 4476

This paper has been typeset from a $\text{\TeX}/\text{\LaTeX}$ file prepared by the author.